

## QUANTITATIVE ANALYSIS OF THE OSCILLATION SPECTRUM OF $\eta$ BOOTIS

D. B. GUENTHER

Department of Astronomy and Physics, Saint Mary's University, Halifax, NS B3H 3C3, Canada

Received 2004 January 11; accepted 2004 May 6

### ABSTRACT

We analyze the recent ground-based  $p$ -mode oscillation observations of  $\eta$  Boo by Kjeldsen and his collaborators using a large and dense grid of stellar model oscillation spectra parameterized by mass, age, and metallicity. The differences between the model and observed oscillation spectra are quantified by a  $\chi^2$  formulation. Based on the seismic data alone we determine two possible solutions for  $\eta$  Boo's mass, age, and metallicity. One solution exhibits mode bumping and is within  $1\sigma$  of  $\eta$  Boo's observed luminosity, effective temperature, and metallicity, and the other solution does not exhibit mode bumping and is within  $2\sigma$  of  $\eta$  Boo's observed luminosity, effective temperature, and metallicity. We show how mode bumping (also associated with the terms “mixed modes” and “avoided crossings”) can be used to fine-tune the age determination. We also show that the nonadiabatic model frequencies are in better agreement with the observed frequencies than the adiabatic frequencies.

*Subject headings:* stars: individual ( $\eta$  Bootis) — stars: interiors — stars: oscillations

### 1. INTRODUCTION

Over the past decade observers have made remarkable progress in detecting the low-amplitude signature of nonradial oscillations of stars. Although stellar modeling has also improved over the same period, especially in the area of opacities (Iglesias & Rogers 1996), the methodology used to analyze a star with an observed spectrum of nonradial oscillation frequencies has not changed. One begins by constructing a variety of stellar evolutionary tracks that have masses and compositions close to currently accepted values. Sometimes other parameters are also varied, such as the mixing-length parameter. Those models along the tracks that fall within the target star's observed position in the H-R diagram are selected and their nonradial oscillation mode frequencies computed. The frequencies of the modes are matched to the observed modes and a subjective assessment is made as to how good the match is. If the match is good, one concludes that the corresponding model is a close match to the structure of the star. The methodology suffers a number of limitations that include the following:

1. The models are coarsely spaced, and as a consequence the corresponding oscillation spectra are themselves coarsely spaced, making it difficult, if not impossible, to interpolate between the spectra to determine optimum model parameters. Basically, one cannot follow trends in the individual mode frequencies as a function of mass, age, or composition. This is especially true for oscillation spectra that have mixed modes, i.e., irregularly spaced modes.

2. The quality of the match is commonly assessed by eyeballing echelle-style plots where the frequency of the mode is plotted against the frequency of the mode modulo the large frequency separation. The difference between the observed and model spectrum are not quantified in any way.

3. The model selection itself is based on the star's H-R diagram position and not on the observed oscillation spectrum; hence, the set of models selected for pulsation are biased toward existing observational constraints. The analysis may not include all possible models that have closely matching oscillation spectra.

4. For evolved stars the frequency spacings of the  $p$ -modes are significantly perturbed from the regular picket-fence-like spacing predicted by asymptotic theory, so much so that identifying and matching modes by eye in an unbiased yet systematic manner is difficult.

In order to address these and other issues, Guenther & Brown (2004) developed a new strategy (hereafter referred to simply as the QDG method for “quantified dense grid” method) to analyze nonradial oscillation data. In their method they compare the star's spectrum one by one to the oscillation spectra from a very dense multiparameter grid of stellar models. The differences between the model and the observed spectra are quantified by a simple  $\chi^2$  formulation, where minima in  $\chi^2$  correspond to model spectra that match the observed spectrum the best. The grid is fine enough and the parameter space large enough to ensure that all standard stellar models are given equal consideration. The grid is also fine enough to allow interpolation in the model parameters. Guenther & Brown (2004) have tested the method with positive results on the Sun and  $\alpha$  Cen A.

A key component of our strategy is to isolate how well the oscillation spectrum by itself constrains the models independent of the other observable constraints, such as mass, luminosity, composition, and effective temperature. This enables us to better judge the quality of the oscillation spectrum. We do not ignore the nonoscillation constraints but also compute  $\chi^2_{\text{model}}$ , which quantifies how well the other observable constraints fit the models. If the oscillation data and the other observable constraints are consistent with each other, the location of the minima in the oscillation  $\chi^2$  and the model  $\chi^2$  should coincide within the uncertainties. If the location of the minima in the model and oscillation  $\chi^2$  do not match, then we must investigate further why they do not match: reexamining the oscillation data, reexamining the nonoscillation observables, and, of course, reexamining the analysis stream. In the classical approach to analyzing the oscillation spectrum, one typically examines only models within the uncertainty box specified by the nonoscillation observables; hence, one never learns whether or not the oscillation data actually fit better models that lie outside the uncertainty box.

Recently, Kjeldsen et al. (2003) combined data from both equivalent width and Doppler velocity observations of the  $p$ -mode spectrum of  $\eta$  Boo to identify 21  $l = 0, 1$ , and 2  $p$ -mode frequencies. From existing stellar models we know that  $\eta$  Boo is more massive than the Sun by half and has nearly or completely exhausted its core of hydrogen fuel. From the perspective of asteroseismology  $\eta$  Boo is an especially interesting star because it is in an advanced phase of evolution; hence, its oscillation spectrum should show signs of mixed modes.

Mixed modes are oscillation modes that have  $g$ -mode-like characteristics in the interior and  $p$ -mode-like characteristics near the surface. An oscillation spectrum containing mixed modes is easily identified by the irregular frequency spacings between adjacent modes. Mixed modes occur when the upper range of frequencies (lowest radial order) of the  $g$ -mode spectrum encroaches on the lower range of frequencies (also lowest radial order) of the  $p$ -mode spectrum. Because  $g$ -modes are effectively trapped inside the inert helium core of post-main-sequence stars, the evolution of their spectrum is governed by the ever increasing mass of the helium core. One by one the  $g$ -modes cross through the  $p$ -modes, first affecting the lowest radial order  $p$ -modes then higher order  $p$ -modes as the helium core grows and the  $g$ -mode spectrum spreads to higher frequencies.

Christensen-Dalsgaard et al. (1995), Guenther & Demarque (1996), and most recently Di Mauro et al. (2003) all note the existence and stress the significance of mixed modes (also identified by the terms “mode bumping” and “avoided crossings”) in their conventional asteroseismic analyses of  $\eta$  Boo. Unfortunately, they are unable to use the mode bumping to any advantage in their modeling of the star because their grids of models are too coarse and the oscillation data not yet of high enough quality.

We present in this paper a test of our new analysis strategy on  $\eta$  Boo and its 21 observed  $p$ -mode frequencies. We compare our results to the conventional analysis of Di Mauro et al. (2003), whose analysis is of the highest standard. We are able to show that the QDG method is able to extract from the oscillation data more quantified information about  $\eta$  Boo than the conventional method. Even though the primary purpose of the paper is to describe the application of the QDG method to an evolved field star, we also take advantage of the dense grid of models to show in detail the effects of mode bumping on the frequency spectrum of a star as it evolves.

## 2. OBSERVATIONAL CONSTRAINTS

For our analysis of  $\eta$  Boo we use the observational constraints on composition, luminosity, and effective temperature adopted by Di Mauro et al. (2003). We also accept without modification the  $p$ -mode frequency determinations of Kjeldsen et al. (2003), which were also used by Di Mauro et al. (2003).

The star  $\eta$  Boo (HD 5235) is nearby ( $\pi_{\text{Hipparcos}} = 88.17 \pm 0.75$  mas), with spectral type G0 IV star. Following Di Mauro et al. (2003), we take the luminosity of  $\eta$  Boo to be  $L/L_{\odot} = 9.02 \pm 0.22$  and its effective temperature to be  $T_{\text{eff}} = 6028 \pm 45$  K. The star is believed to be metal-rich, having approximately twice the metal abundance of the Sun,  $[\text{Fe}/\text{H}] = 0.305 \pm 0.051$ . We therefore take  $Z = 0.04 \pm 0.005$ .

The oscillation spectrum of  $\eta$  Boo determined by Kjeldsen et al. (2003) was obtained by combining four separate ground-based observational sets, two of which are based on Kjeldsen’s equivalent width measurements and two of which are based

on Doppler shift measurements, one by Kjeldsen and one by Brown et al. (1997). The oscillation mode frequencies, when plotted in an echelle diagram, fall along three distinct vertical curves corresponding to  $l = 0, 1$ , and 2  $p$ -modes. Two  $l = 1$  modes, 749.3 and 753.4  $\mu\text{Hz}$ , if distinct and real are evidence for mode bumping since the observed average large spacing is approximately 41  $\mu\text{Hz}$ .

Based on the scatter seen in their echelle diagram (Fig. 9 of Kjeldsen et al. 2003), we adopt their  $2\sigma$  frequency uncertainties for our analysis. The observational uncertainty for each mode was derived by Kjeldsen et al. from the signal-to-noise ratio of the mode’s peak in the power spectrum.

## 3. MODEL GRID

The QDG method (Guenther & Brown 2004) employs dense and extensive grids of stellar models. The resolution of the grid (i.e., grid density) is set by the need to be able to compute oscillation spectra of models in between mass-age grid points using linear interpolation. The models themselves are constructed using the Yale stellar evolution code (historically referred to as YREC; Guenther et al. 1992). The physics of the models, described in Guenther & Brown (2004), are current and include OPAL98 (Iglesias & Rogers 1996) and Alexander & Ferguson (1994) opacity tables, Lawrence Livermore equation-of-state tables (Rogers 1986; Rogers et al. 1996), and nuclear reaction cross sections from Bahcall et al. (2001). For all the models of  $\eta$  Boo considered here, diffusion is turned off. Our existing diffusion implementation, based on the Bahcall et al. (1995) formulation, is not adequate to follow correctly the effects of diffusion in thin convective envelopes (Morel & Thévenin 2002; Sills & Deliyannis 2000). When we include diffusion (gravitational settling) in our models of stars that have thin convective envelopes, we find that all of the helium and heavy elements are drained out of the convective envelope, a result that is inconsistent with observation. To improve the model of the outer layers it will be necessary minimally to follow the effects of levitation (i.e., radiative accelerations), which are not included in our diffusion computation, and the effects of the high convective velocities that are associated with shallow convective envelopes. Michaud and his collaborators have carried out much more physically realistic diffusion models (Richer et al. 2000). Accurate asteroseismic observations may be able to discern not only the limitations of our current models but also guide us in refining our models of the outer layers.

For a given composition and mixing-length parameter, evolutionary tracks from 0.81 to 2.0  $M_{\odot}$  spaced 0.01  $M_{\odot}$  apart are constructed. Along each track, equally spaced in  $\log T_{\text{eff}}$  and  $\log L/L_{\odot}$ , the  $l = 0, 1, 2$ , and 3  $p$ -mode oscillation spectra of the models are computed. The computed frequencies of the modes range from the lowest  $p$ -mode frequency at  $n = 1$  to the acoustic cutoff frequency.

We have over the past year constructed grids for a variety of compositions. For this study on  $\eta$  Boo, the  $(X, Z) = (0.71, 0.03)$  and  $(0.71, 0.04)$  grids are used. We note that the Di Mauro et al. models were computed at  $X = 0.70$ . Each composition grid consists of 10,000–20,000 models.

Guenther’s nonradial nonadiabatic stellar pulsation program (Guenther 1994) was used to compute the adiabatic and nonadiabatic  $p$ -mode frequencies of each of the models in the grid. The code uses the Henyey relaxation method to solve the linearized nonradial nonadiabatic pulsation equations. The nonadiabatic component includes radiative energy gains and

losses as formulated in the Eddington approximation but does not include coupling of convection to the oscillations.

#### 4. QDG METHOD

We wrote a computer program to search through the grids of model oscillation spectra and seek out spectra that closely match the observed spectrum. The difference between the observed and model spectrum is quantified by the following  $\chi^2$  definition:

$$\chi^2 \equiv \frac{1}{N} \sum_{i=1}^N \frac{(\nu_{\text{obs},i} - \nu_{\text{mod},i})^2}{\sigma_{\text{obs},i}^2 + \sigma_{\text{mod},i}^2},$$

where  $\nu_{\text{obs},i}$  is the observed frequency for the  $i$ th mode,  $\nu_{\text{mod},i}$  is the corresponding model frequency for the  $i$ th mode,  $\sigma_{\text{obs},i}$  is the observational uncertainty for the  $i$ th mode,  $\sigma_{\text{mod},i}$  is the model uncertainty for the  $i$ th mode, and  $N$  is the total number of matched modes. Details of the searching and mode matching procedure are described in Guenther & Brown (2004). This model uncertainty originates primarily from uncertainties in the modeling of the surface layers of the stars and increases from a tenth of a percent to a half a percent as the frequencies of the modes approach the acoustic cutoff frequency (see Fig. 1 of Guenther & Brown 2004). This is clearly a systematic effect. Rather than trying to correct for the shift, we choose at this time to treat it as a statistical uncertainty so that we can more easily recognize similar systematic shifts in other stars. We note that the irregularities in the curves in Figure 1 of Guenther & Brown correspond to observational rather than model uncertainties.

The search program not only looks at the spectra of models at mass-age grid points but also looks at interpolated spectra between the model grid points. Two-dimensional linear interpolation is performed in mass and age to obtain a 10-fold increase in effective grid resolution along each dimension. The higher effective resolution enables one to follow more smoothly the changes in  $\chi^2$ , for example, as one approaches, in mass and age, a model whose spectrum closely matches the observed spectrum. The total number of model spectra actually searched within each composition grid is approximately 1–2 million.

Although the search program computes  $\chi^2$  values for all of the models, only low values of  $\chi^2$  are normally output. For convenience the lowest value of  $\chi^2$  along each mass track is identified and output by the code to a separate file. When  $\chi^2$  falls below a specified threshold the search code will also output the interpolated spectra of the model.

In addition, the search program computes  $\chi_{\text{model}}^2$  from the known model observables, such as mass, luminosity, effective temperature, and composition. For this analysis of  $\eta$  Boo, we use

$$\chi_{\text{model}}^2 \equiv \frac{1}{3} \left[ \frac{(Z_{\text{obs}} - Z_{\text{mod},i})^2}{\sigma_Z^2} + \frac{(T_{\text{obs}} - T_{\text{mod},i})^2}{\sigma_T^2} + \frac{(L_{\text{obs}} - L_{\text{mod},i})^2}{\sigma_L^2} \right],$$

where  $Z$  and  $\sigma_Z$  are the mass fraction metal abundance and its uncertainty,  $T$  and  $\sigma_T$  are the effective temperature and its uncertainty, and  $L$  and  $\sigma_L = 0.22 L_{\odot}$  are the luminosity and its uncertainty.

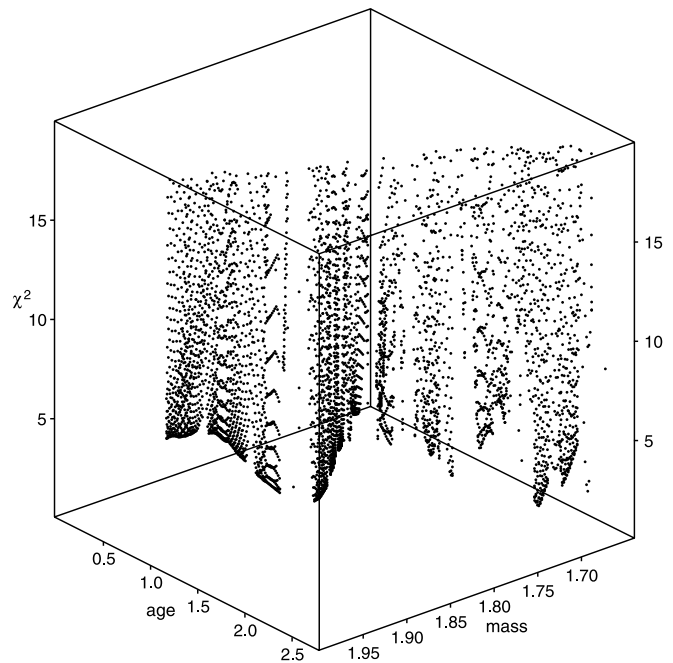


FIG. 1.—Values of  $\chi^2 < 20$  for  $\eta$  Boo are plotted as a function of mass and age. Each point corresponds to a unique stellar model. The value of  $\chi^2$  is determined from nonadiabatic model frequencies for models with  $Z = 0.04$ .

For main-sequence stars like the Sun we find that  $\chi^2$  varies smoothly as a function of mass, age,  $Z$ ,  $T_{\text{eff}}$ , and  $L/L_{\odot}$ , dipping to well-defined minima. For more evolved stars our tests show that the  $\chi^2$  curves are not as smoothly varying as for main-sequence stars, primarily because of mode bumping. The mode frequencies can change abruptly between adjacent models in the grid because of mode bumping, and as a consequence, the computed  $\chi^2$  will also change abruptly. The abrupt changes can only be resolved by increasing the grid resolution. In anticipation of future studies on post-main-sequence stars, we are in the process of constructing higher resolution grids.

#### 5. BEST-FITTING MODEL SPECTRA

Of all of the models in the grid, only a small fraction of the models have oscillation spectra that are a relatively close match, where we loosely define a close match to have  $\chi^2 < 100$ . In the case of  $\eta$  Boo this corresponds to models whose oscillation frequencies are within approximately  $\pm 2 \mu\text{Hz}$  of the observed frequencies. The search program failed to find any models that were a close match to all 21 observed  $p$ -modes. The search program, though, did find close matches for 20 of the 21  $p$ -modes, with either the  $l = 1$  749.3  $\mu\text{Hz}$  mode or the  $l = 1$  753.4  $\mu\text{Hz}$  mode failing to be matched.

In Figure 1 we show a three-dimensional plot of  $\chi^2$  versus mass and age for the  $Z = 0.04$  model grid. The values of  $\chi^2$  were calculated from the real component of the nonadiabatic frequencies. The models that have spectra that are a close match to the observed spectrum of  $\eta$  Boo lie close to a two-dimensional sheet (only the lower portion of this sheet is shown in Fig. 1). Even by only evoking the loose constraint that  $\chi^2 < 100$ , one significantly constrains the mass and ages of the possible models.

To simplify more detailed analysis of the  $\chi^2$  results, we project the three-dimensional plot of  $\chi^2$  versus mass and age onto the age versus  $\chi^2$  plane and only plot the lowest values of  $\chi^2$  for each age. The result is shown in Figure 2, where we also

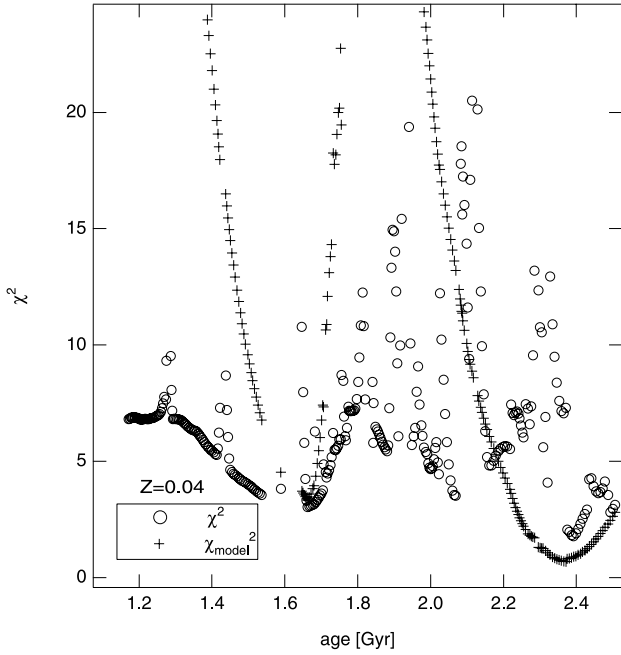


FIG. 2.—Values of  $\chi^2$  determined from the oscillation spectra and values of  $\chi_{\text{model}}^2$  determined from the luminosity, effective temperature, and metallicity of the models are plotted as a function of age. Only the lowest values of  $\chi^2$  are plotted.

show the model  $\chi_{\text{model}}^2$  values. These values are only computed for models with  $\chi^2 < 100$ . Recall that  $\chi_{\text{model}}^2$  is a measure of how well the corresponding model's luminosity, effective temperature, and metal abundance match the observed values for  $\eta$  Boo and that  $\chi^2$  is a measure of how well the corresponding model's oscillation spectrum matches the observed spectrum, independent of the luminosity, effective temperature, and metallicity of the model. The oscillation  $\chi^2$  dips below 5 near 1.65, 2.1, and 2.4 Gyr. The corresponding model  $\chi_{\text{model}}^2$  dips below 5 near 1.65 and 2.4 Gyr but not 2.1 Gyr. If the

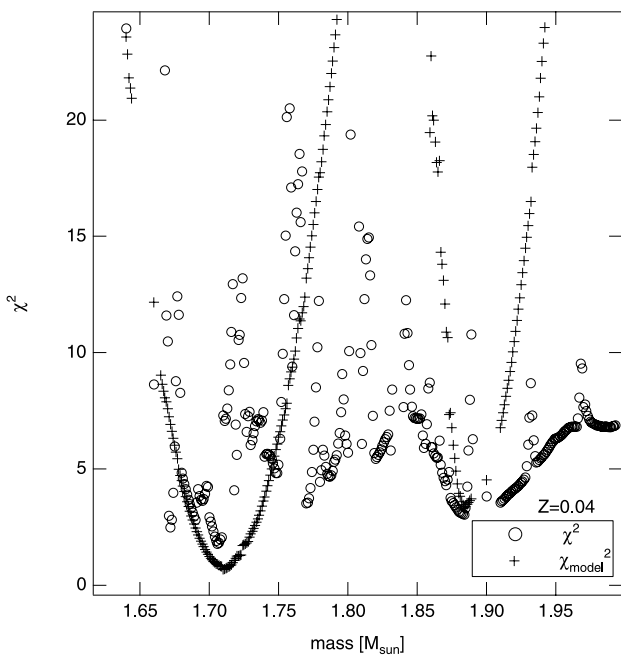


FIG. 3.—Values of  $\chi^2$  and  $\chi_{\text{model}}^2$  are plotted as a function of mass.

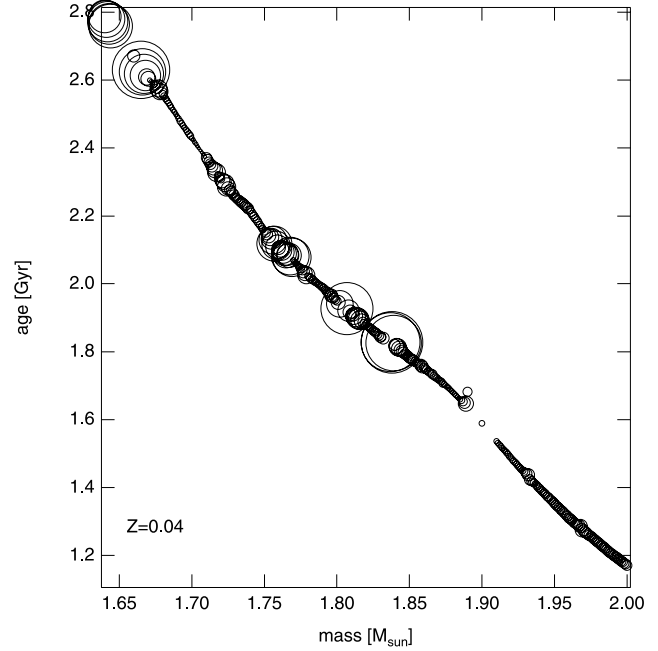


FIG. 4.—Lowest values of  $\chi^2$  shown in Fig. 1 are projected onto the mass-age plane. The size of the symbol is scaled to the size of  $\chi^2$ , with the smallest symbols corresponding to  $\chi^2 < 5$  and the largest symbols to  $\chi^2 > 50$ .

observed oscillation spectrum is valid, then we expect that models that match the spectrum best should also fall within the observed constraints on  $L$ ,  $T_{\text{eff}}$ , and  $Z$ . In the case of  $\eta$  Boo, we clearly have consistent results in two regions, one at 1.65 Gyr and the other at 2.4 Gyr.

Next we project the three-dimensional plot of  $\chi^2$  versus mass and age onto the mass versus  $\chi^2$  plane and only plot the lowest values of  $\chi^2$  for each mass, as shown in Figure 3. The two regions of best-fitting spectra and  $L$ ,  $T_{\text{eff}}$ , and  $Z$ , corresponding to minima in  $\chi^2$  and  $\chi_{\text{model}}^2$ , respectively, are clearly defined, one near  $1.71 M_{\odot}$  (which corresponds to the minimum near 2.4 Gyr) and the other near  $1.88 M_{\odot}$  (which corresponds to the minimum near 1.65 Gyr).

Finally, we project the lowest values of  $\chi^2$  onto the mass versus age plane to obtain Figure 4. In Figure 4 the size of the plot symbol is proportional to the value of  $\chi^2$ , with the smallest circles corresponding to  $\chi^2 < 5$  and the largest circles corresponding to  $\chi^2 > 50$ . As previously noted, by constraining the models to match closely the observed spectrum one restricts the allowed mass and ages of the models, as shown in Figure 4. We note that if we were to project all  $\chi^2 < 100$  points onto the mass-age plane in Figure 4, we would still obtain the well-defined mass-age constraint.

We computed  $\chi^2$  values for models with  $Z = 0.03$ . In Figure 5 we plot  $\chi^2$  versus mass for both the  $Z = 0.03$  and  $Z = 0.04$  models. We also plot the  $\chi_{\text{model}}^2$  values corresponding to the  $Z = 0.03$  models. The  $Z = 0.04$  models have lower  $\chi^2$  than the  $Z = 0.03$  models. Furthermore, only the models near  $1.65 M_{\odot}$  have  $\chi_{\text{model}}^2$  values below 20.<sup>1</sup> This implies not only that the oscillation spectra of the  $Z = 0.04$  models fit  $\eta$  Boo's observed spectrum better than the  $Z = 0.03$  models, but also that the corresponding model parameters of  $L$ ,  $T_{\text{eff}}$ , and  $Z$  are a better match to the observed values.

<sup>1</sup> Because we have assumed that  $Z = 0.04 \pm 0.005$  for  $\eta$  Boo,  $\chi_{\text{model}}^2$  for a  $Z = 0.03$  model will be +1.33 larger than the same model at  $Z = 0.04$ .

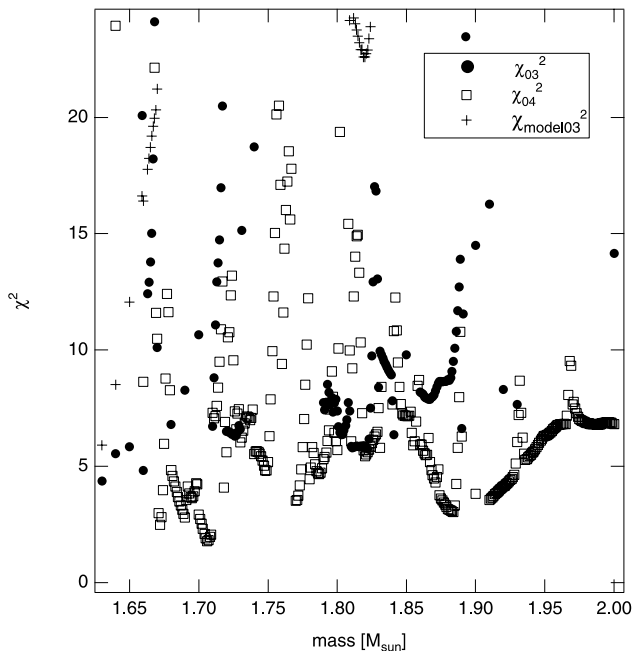


FIG. 5.—Values of  $\chi_{04}^2$ ,  $\chi_{03}^2$ , and  $\chi_{\text{model}03}^2$  are plotted as a function of mass, where  $\chi_{04}^2$  is computed from the frequency spectrum of models with  $Z = 0.04$ ,  $\chi_{03}^2$  is computed from the frequency spectrum of models with  $Z = 0.03$ , and  $\chi_{\text{model}03}^2$  is computed from the luminosity, effective temperature, and metallicity of models with  $Z = 0.03$ .

We also carried out all our oscillation spectra comparisons using nonadiabatic model frequencies. The nonadiabatic nonradial oscillation mode computation has only been tested, to date, for the Sun, where it is well established that the nonadiabatic model frequencies fit the Sun's observed spectrum better than the adiabatic model frequencies. Here we are considering a more massive star in a more advanced phase of evolution and with probably a very shallow convection zone. To test whether or not the nonadiabatic computation also provides a better fit for  $\eta$  Boo, we compare in Figure 6

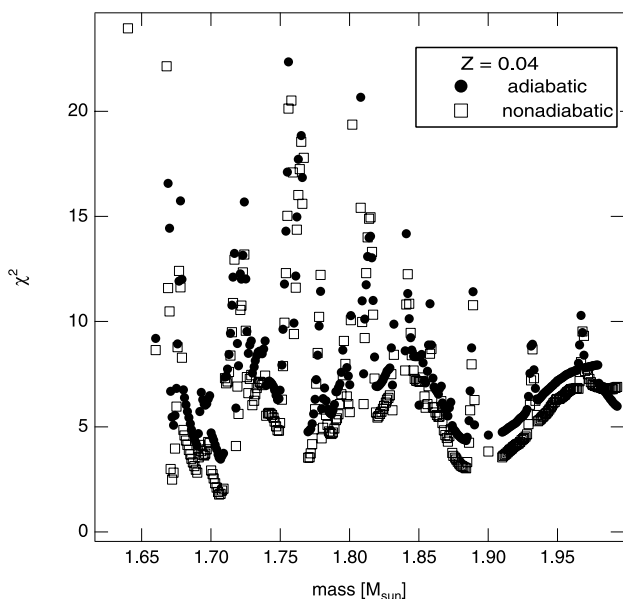


FIG. 6.—Values of  $\chi^2$  computed from adiabatic and nonadiabatic model frequencies are compared as a function of model mass.

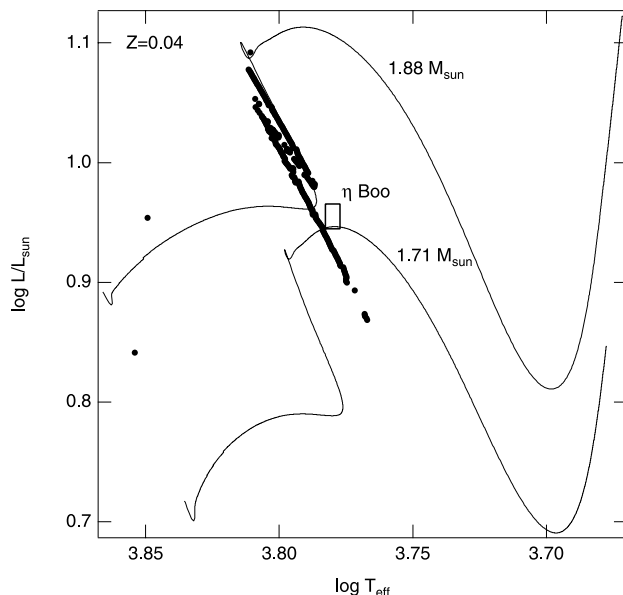


FIG. 7.—H-R diagram showing the evolutionary tracks for a  $1.71 M_{\odot}$  and a  $1.88 M_{\odot}$  model, both with  $Z = 0.04$ . The error box marks  $\eta$  Boo's position in the H-R diagram. The filled symbols mark the location of all models within the  $Z = 0.04$  grid that have  $\chi^2 < 100$ .

$\chi^2$  values computed from adiabatic frequencies to  $\chi^2$  values computed from nonadiabatic frequencies. The nonadiabatic mode frequencies for models near  $1.71$  and  $1.88 M_{\odot}$  have lower  $\chi^2$  and are clearly a better fit to the observed frequencies than the adiabatic mode frequencies. We note that because  $\eta$  Boo has a very shallow convective envelope with high convective velocities, the nonadiabatic corrections due to turbulence, which are not included in our nonadiabatic formulation, may have a significant impact on mode amplitudes and lifetimes (the imaginary component of the frequency). The layer is small and hence should not affect the real component of the frequencies used here. Regardless, if discrepancies between our models and more detailed observations were seen, we would first look to this limitation in our models.

In Figure 7 we plot the evolutionary tracks for the  $1.71$  and the  $1.88 M_{\odot}$  models, which correspond to the two model grid masses closest to the local minima in  $\chi^2$  (see Figs. 3 and 4). The actual minima occur at interpolated model grid points. The  $1\sigma$  error box for  $\eta$  Boo's H-R diagram position is plotted. Filled circles denote the position of models with  $\chi^2 < 100$ . We see here that the two regions where  $\chi^2$  and  $\chi_{\text{model}}^2$  are both less than 5 correspond to two distinct phases of evolution, that is, main-sequence evolution for the  $1.88 M_{\odot}$  model and subgiant branch evolution for the  $1.71 M_{\odot}$  model. The oscillation spectra of models from these two regions are distinct. The subgiant models have an inert helium core that traps  $g$ -modes and produces mixed or bumped  $p$ -modes. Their frequency spectra are characterized by irregularly spaced modes. Mode bumping in the main-sequence models is not as advanced and only the very lowest radial order modes (not observed) are mixed modes. Their frequency spectra are characterized by regularly spaced modes.

The two local minima in  $\chi^2$  for the  $Z = 0.04$  grid are located at interpolated mass-age points of  $1.706 M_{\odot}$ , 2.393 Gyr and  $1.884 M_{\odot}$ , 1.663 Gyr. In Figures 8 and 9 we plot the frequency spectra for these two model solutions along with the observed frequencies in an echelle diagram. The error bars on

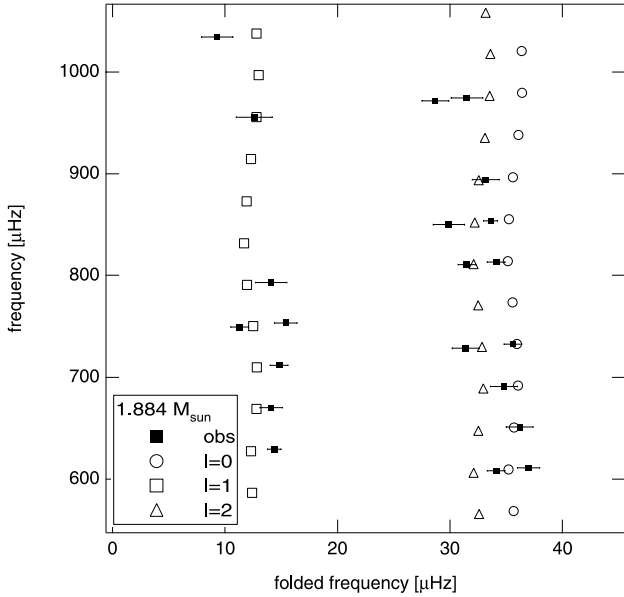


FIG. 8.—Echelle diagram comparing the  $Z = 0.04$ ,  $1.884 M_{\odot}$  model non-adiabatic frequencies to the observed frequencies for  $\eta$  Boo. The error bars on the observations are  $2 \sigma$  values. The folding frequency is  $41 \mu\text{Hz}$ .

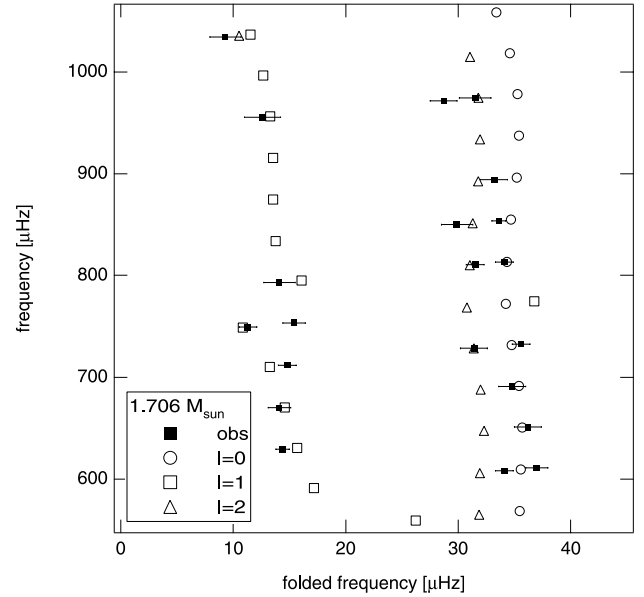


FIG. 9.—Echelle diagram comparing the  $Z = 0.04$ ,  $1.706 M_{\odot}$  model non-adiabatic frequencies to the observed frequencies for  $\eta$  Boo. The error bars on the observations are  $2 \sigma$  values. The folding frequency is  $41 \mu\text{Hz}$ .

the observed frequencies are  $2 \sigma$  values. The folding frequency is  $41 \mu\text{Hz}$ . In Figure 8, corresponding to the main-sequence model, the oscillation frequencies of the model lie along three distinct vertical curves corresponding to  $l = 0, 1$ , and  $2 p$ -modes. In Figure 9, corresponding to the subgiant branch model, the oscillation frequencies also lie along three distinct curves, but between  $750$  and  $800 \mu\text{Hz}$  along the  $l = 1$  curve, one of the modes is bumped far off the  $l = 1$  curve onto the  $l = 0$  curve. We discuss the significance of this in § 6. Both fits look good. The  $1.706 M_{\odot}$  model has  $\chi^2 = 1.7816$  and the  $1.884 M_{\odot}$  model has  $\chi^2 = 3.0259$ .

We stated earlier that the search program failed in all cases to match all 21 observed  $p$ -modes, matching only 20 of the 21 modes. The two modes that could not be simultaneously matched are the  $l = 1$  modes at  $749.3$  and  $753.4 \mu\text{Hz}$ . The two modes are separated by much less than the average large spacing. Some possible interpretations are as follows:

1. One or both of the two modes are erroneous.
2. One of the modes is a bumped  $l = 1$  mode.
3. One of the modes is a bumped  $l = 2$  mode.
4. One of the modes is an  $l = 3$  mode.

Needless to say, additional observations are required to confirm the existence of the two modes. We note that the two modes were identified in two of the four distinct data sets used by Kjeldsen et al. (2003). If the mode is an  $l = 3 p$ -mode, then we expect that other  $l = 3$  modes would also be observable. If one of the two modes is a bumped mode, then we can rule out the main-sequence solution at  $1.884 M_{\odot}$  because its oscillation spectrum does not contain any bumped modes in the observed frequency range.

## 6. EVOLUTION OF BEST-FITTING MODEL

The QDG method relies heavily on the resolution of the grid. If the grid is too coarse then it is possible to miss or skip over important and subtle features observed in the oscillation spectrum of a star, such as mode-bumping details. The QDG method quickly and unambiguously identifies models that

have closely matching oscillation spectra. Once such models have been identified, more refined models can be constructed to study the star's oscillation spectrum in more detail. Our analysis of  $\eta$  Boo in § 5 using the QDG method left us with two distinct possible solutions for  $\eta$  Boo.

The fact that  $\eta$  Boo appears to have bumped modes has already been noted in the literature by Christensen-Dalsgaard et al. (1995) and Guenther & Demarque (1996). The existence of mode bumping was further commented on by Di Mauro et al. (2003). Although all of these papers conclude that with more accurate observations one could use the mode bumpings to further constrain the models, none of the authors describe exactly how the bumped modes can be used to enhance the analysis of  $\eta$  Boo. In this section we show by the example of  $\eta$  Boo one way in which the mode bumpings can be used to fine-tune our models. We stress that this is a demonstration only since the evidence for mode bumping is tentative.

We evolved a  $Z = 0.04$ ,  $1.706 M_{\odot}$  model from the zero-age main sequence (ZAMS) to the giant branch (GB) with 4 times the temporal resolution as used in our grid. We then computed oscillation spectra of the models along this track.

In Figures 10, 11, and 12 we plot the  $l = 0, 1$ , and  $2 p$ -mode frequencies of the  $1.706 M_{\odot}$  models as they evolve from the ZAMS to the GB. As the models evolve and their radii during most stages of evolution increase, the frequency spacing between the models decreases since the frequency spacing to first order is inversely proportional to the  $3/2$  power of the radius. The modes range from  $n = 1$  to the acoustic cutoff frequency. The mode frequencies are plotted against  $\lambda$  to better follow the evolution of the modes. The term  $\lambda$  is a dimensionless quantity that approximates the arc length distance from the ZAMS to the model's position along its evolutionary track in the H-R diagram. It is computed by integrating  $d\lambda$  defined by  $d\lambda^2 \propto [d(\log L/L_{\odot})]^2 + [c d(\log T_{\text{eff}})]^2$  along the evolutionary path of the star in the H-R diagram (from its ZAMS location to its current location). The models in our grids are computed with  $c = 10$ , a constant that can be adjusted according to the specific evolutionary phase being studied;  $\lambda$  scales nonlinearly

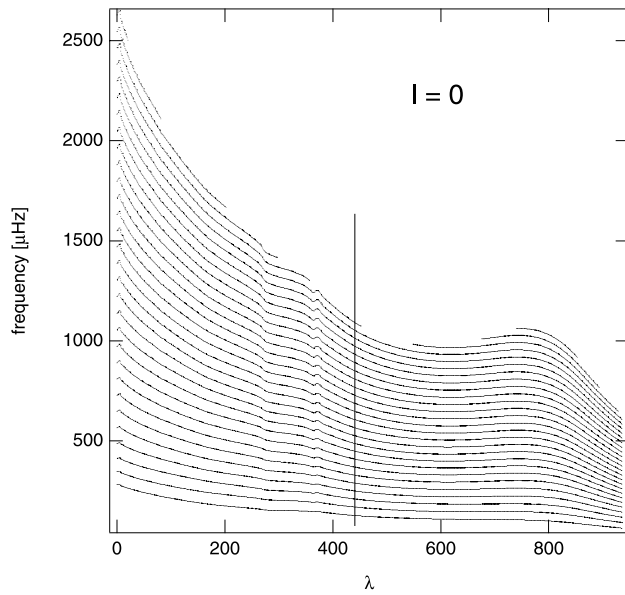


FIG. 10.—Nonadiabatic  $l = 0$   $p$ -mode frequencies for the models along the  $1.706 M_{\odot}$ ,  $Z = 0.04$  evolutionary track are plotted as a function of  $\lambda$ , where  $\lambda$  is a parameter, defined in the text, that is related to the arc length distance the star travels in an H-R diagram (see Fig. 13). The vertical line corresponds to the model that has the lowest  $\chi^2$ .

with age. By using  $\lambda$  we can select models that are relatively equally spaced along the evolutionary track and thereby better resolve changes in the star's structure and its effect on the  $p$ -mode frequencies during rapid phases of evolution, such as the subgiant branch phase. For reference, the evolutionary track of the  $1.706 M_{\odot}$  model with values of  $\lambda$  identified along the track is shown in Figure 13. The error box of  $\eta$  Boo and the location of the minimum  $\chi^2$  model are indicated. In Figures 10, 11, and 12 a vertical line is drawn through the modes where  $\chi^2$  for  $\eta$  Boo reaches a minimum. The first couple of avoided crossing ridges are labeled “g1,” “g2,” etc., in the  $l = 1$  and  $l = 2$  plots.

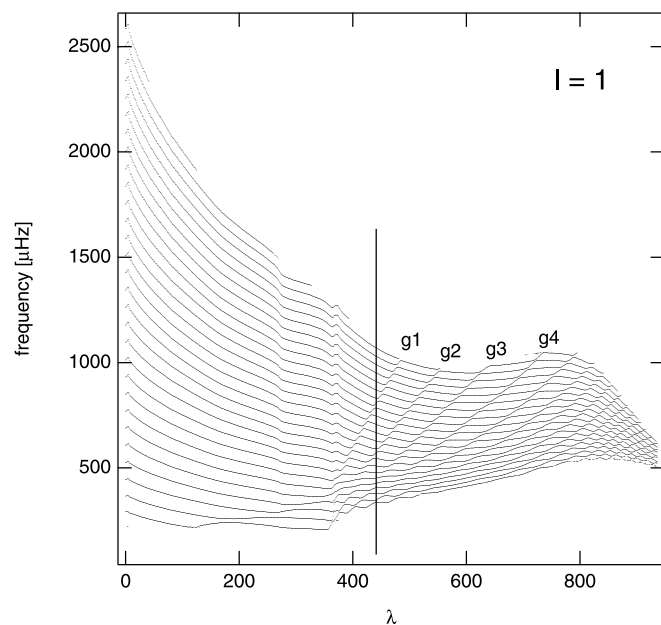


FIG. 11.—Similar to Fig. 10, except for  $l = 1$   $p$ -mode frequencies.

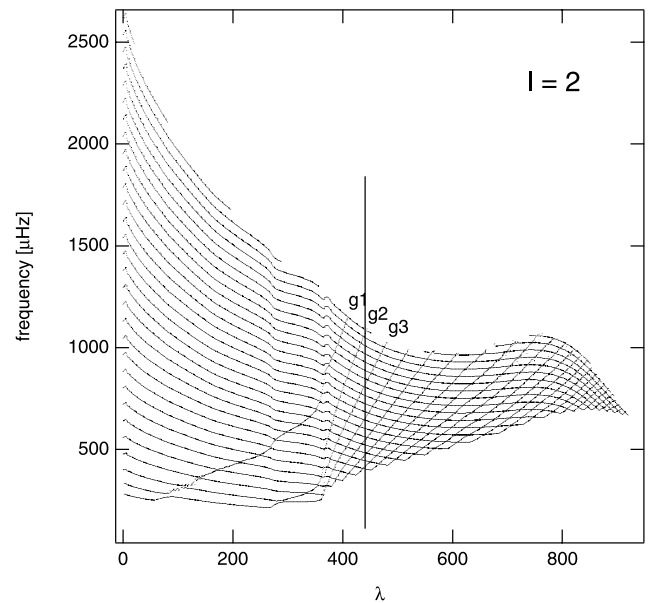


FIG. 12.—Similar to Fig. 10, except for  $l = 2$   $p$ -mode frequencies.

To the left of the g1 avoided-crossing ridge, the modes are pure  $p$ -modes with no  $g$ -mode component. Modes between the g1 ridge and the g2 ridge are mixed modes, with their centermost radial node having the phase characteristics of a  $g$ -mode (Unno et al. 1989) and the rest of their nodes having  $p$ -mode phase characteristics. Note that throughout our discussion of mode bumping we use the nomenclature of Scuflaire (1974), where the radial order  $n$  is computed as the difference between the number of  $p$ -mode-like nodes and the number of  $g$ -mode-like nodes. This nomenclature provides a unique radial-order identification for most modes. In the region between the g1 and g2 ridges, for example, an  $n = 3$  mode has one  $g$ -mode-like node,  $n_G = 1$ , and four  $p$ -mode-like nodes,

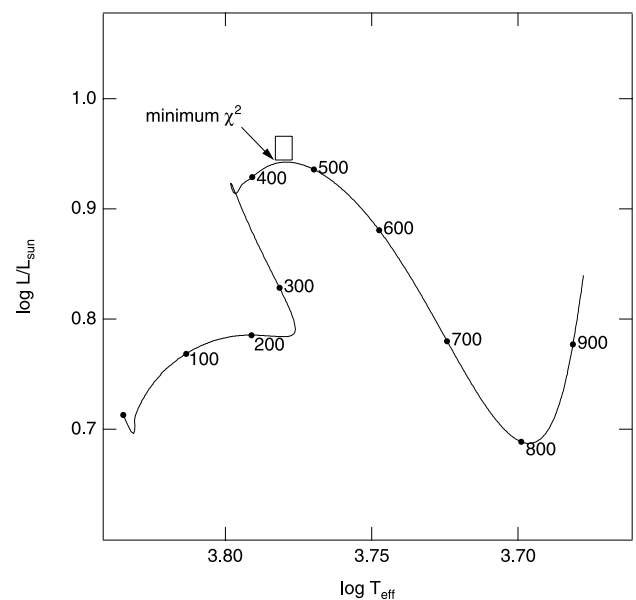


FIG. 13.—H-R diagram showing the evolution of a  $1.706 M_{\odot}$ ,  $Z = 0.04$  model. The location of  $\eta$  Boo and the model with the minimum  $\chi^2$  are indicated. Numbers label the corresponding values of  $\lambda$  along the track.

$n_p = 4$ , where  $n \equiv n_p - n_G$ . As the star evolves,  $n_G$  increases and the  $g$ -mode mixing extends to higher frequencies.

Figure 11 shows that as the star evolves its acoustic cutoff frequency decreases. We also see that as the star evolves its nonradial (i.e.,  $l > 0$ )  $n = 1$  mode frequency increases.

In Figure 14 we show an enlarged section of Figure 11 ( $l = 1$ ). The avoided-crossing ridges are now fully resolved. Following a mode as  $\lambda$  increases, the frequency of a mode decreases as the radius of the star increases. Nearing an avoided-crossing ridge, the mode's frequency quickly increases (is bumped by a mode below) and approaches the frequency of the next higher (frequency) mode. It narrowly avoids crossing through the frequency of the next mode and veers sharply away, resuming its move toward lower frequencies. The next higher mode is now itself bumped and quickly increases in frequency. The avoided-crossing ridges propagate in this manner upward to higher frequencies. As the mode evolves through an avoided-crossing ridge the character of the nodes changes while the radial order remains constant: the number of  $g$ -mode-like and  $p$ -mode-like nodes both increase by one.

In the region to the left of the  $g1$  ridge the spacing between the modes for a given model is relatively even, and to the right of the  $g1$  ridge the spacing becomes more and more irregular as one crosses more avoided-crossing ridge lines. The frequencies of modes near the avoided-crossing ridges are squeezed together.

Mode bumping adds a unique and identifiable signature to the oscillation spectra of evolved models. Unless a very fine grid of models is computed, the quickly changing frequencies of the modes as they are bumped are difficult to track. This is especially true of the  $l = 2$  modes for stars near main-sequence turnoff, where the avoided-crossing ridge lines are very steep.

Returning to Figure 14 and our analysis of  $\eta$  Boo, the age corresponding to the model with the minimum  $\chi^2$  (2.393 Gyr) is marked by a vertical line. The minimum  $\chi^2$  was determined from the models in our grid and not from the models along the  $1.706 M_\odot$  track. Horizontal lines through the vertical line mark the frequencies of all of the observed  $l = 1$   $p$ -modes. The  $l = 1$  modes fall very close to the model values. The match is not perfect, although shifting to a slightly lower age (2.388 Gyr) does improve the match. The small discrepancy in age (0.005 Gyr) between the best  $\chi^2$  age determined from the model grid and the best age as estimated from Figure 14 is due to the smaller time steps used to construct the  $1.706 M_\odot$  track and represents the approximate age error in these stellar models. It also demonstrates the need for high grid resolutions when tracking and comparing model spectra to observed spectra.

We would expect the two closely spaced  $l = 1$   $p$ -modes in  $\eta$  Boo's observed spectrum to be located in frequency near where an avoided-crossing ridge passes through the spectrum. Extraordinarily, the frequency location of the two closely spaced  $l = 1$   $p$ -modes is indeed very close to where the  $g1$  ridge passes through this model's spectrum. The oscillation spectra fit best a model that not only falls within  $1 \sigma$  of the observed  $L$ ,  $T_{\text{eff}}$ , and  $Z$  values but also has a  $g1$  ridge cutting through the oscillation spectrum very close (within 0.005 Gyr!) to where the two closely spaced  $l = 1$   $p$ -modes are observed. Although this is an exciting result, one notes quite clearly that the observed spacing between these modes is much closer than the models predict.

To summarize, based on Kjeldsen et al. (2003) mode frequencies and our application of the QDG method,  $\eta$  Boo

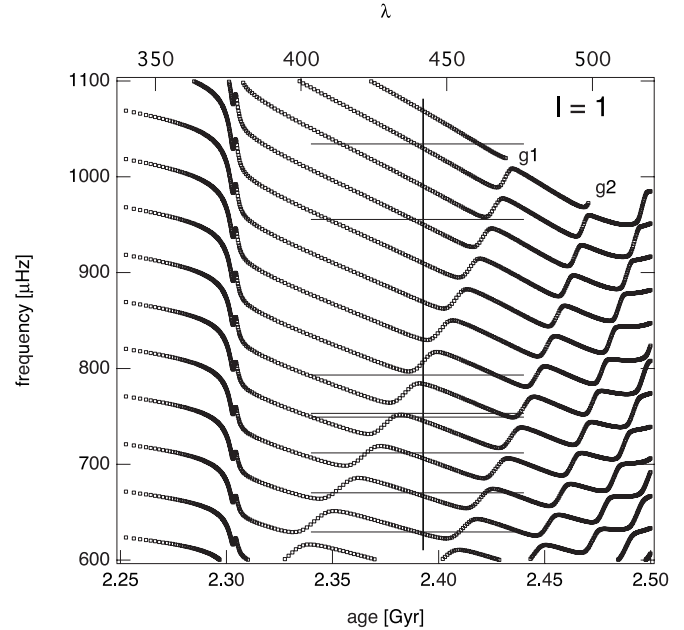


FIG. 14.—Enlarged section of Fig. 11. The vertical line marks the age of the model with the minimum  $\chi^2$ . The horizontal lines mark the frequencies of the observed  $l = 1$   $p$ -modes.

is either a  $Z = 0.04$ ,  $1.71 M_\odot$  star near 2.393 Gyr in age (post-main-sequence phase) or a  $Z = 0.04$ ,  $1.88 M_\odot$  star near 1.663 Gyr in age (late-main-sequence phase). If mode bumping is confirmed, then only the former solution can be valid. Assuming that the uncertainties in the frequencies are approximately  $\pm 1 \mu\text{Hz}$ , we estimate, from Guenther & Brown (2004), that the mass and age determinations are accurate to 3%. Our results are consistent with Di Mauro et al. (2003), who determine a mass range of  $1.64$ – $1.75 M_\odot$ . We obtain a slightly higher age than Di Mauro et al., who get ages ranging from 2.37 to 2.39 Gyr, partly because we have compared the observed frequencies to nonadiabatic model frequencies rather than adiabatic frequencies and partly because our models have a slightly lower helium abundance. The  $1.71 M_\odot$  solution is within  $1 \sigma$  of the observed constraints on luminosity, effective temperature, and metallicity, and the  $1.88 M_\odot$  solution is within  $2 \sigma$ .

The models along the  $1.706 M_\odot$  evolution track have a very thin convective envelope up through the model that best fits the oscillation data. The star is evolving very quickly at this phase of evolution and the convective envelope grows very rapidly afterward, with models only 25 Myr farther along the track having convective envelopes already reaching a depth of 0.81 radius fraction (i.e., a depth that is consistent with the envelope depths of the models of Di Mauro et al.). The models in our grid, which are based on the standard mixing-length approximation, assume a mixing-length parameter ( $\alpha = 1.633$ ) calibrated to models of the Sun using the same basic model physics as used to construct the models in our grid.

## 7. SUMMARY AND CONCLUSIONS

We have compared the oscillation spectra of a wide range of stellar models to the observed oscillation spectrum of  $\eta$  Boo and isolated two potential model solutions, one with  $Z = 0.04$ ,  $M = 1.706 M_\odot$ , age = 2.393 Gyr, and  $\chi^2 = 1.78$ , and the other with  $Z = 0.04$ ,  $M = 1.884 M_\odot$ , age = 1.663 Gyr, and  $\chi^2 = 3.03$ . The  $1.706 M_\odot$  model has exhausted its hydrogen core and is beginning its evolution toward the giant branch.

The  $1.884 M_{\odot}$  model is still on the main-sequence but is approaching hydrogen exhaustion. Uncertainties in the mass and age determinations are estimated to be of the order of 3% based on an uncertainty of  $\pm 1 \mu\text{Hz}$  for the observed frequencies. The  $1.706 M_{\odot}$  model solution is consistent with the findings of Di Mauro et al. (2003).

The solution models, that is, their mass, age, and metallicity, were obtained using only the oscillation modes as constraints. Both solutions, though, are consistent with the observed constraints on luminosity, effective temperature, and metallicity to within  $1 \sigma$  for the  $1.706 M_{\odot}$  model and to within  $2 \sigma$  for the  $1.884 M_{\odot}$  model.

Of the two possible models the  $1.706 M_{\odot}$  is the only valid model if the observed mode bumping in two of the  $l = 1$  modes (at 749 and 753  $\mu\text{Hz}$ ) is real. The lowest order avoided-crossing ridge passes through the frequency spectrum of the  $l = 1$   $p$ -modes for  $1.706 M_{\odot}$  models very near the frequencies of the two suspected bumped modes. None of the frequencies of the  $1.884 M_{\odot}$  model, within the observed range, are bumped.

Our  $1.706 M_{\odot}$  model of  $\eta$  Boo does not have a convection zone, while a slightly more evolved model along the track does. We speculate that  $\eta$  Boo does have a shallow convection zone (under the assumption that its existence is necessary to drive the oscillations) unresolved by our models owing to uncertainties in the mixing-length approximation, the surface abundances, and the low-temperature opacities. This in turn suggests that the nonadiabatic corrections to the frequencies due to turbulence, which are not included in our  $p$ -mode calculation, may be small compared to the nonadiabatic corrections due to radiation, which are included. Needless to say,  $\eta$  Boo offers a critical test for models of stellar convection.

We show for  $\eta$  Boo that the nonadiabatic model frequencies match the observed frequencies better than the adiabatic frequencies. This result supports the physics of the nonadiabatic calculation, which prior to our analysis of  $\eta$  Boo has only been tested on the Sun, where it is known to improve the match between the oscillation frequencies of the solar model and the observations.

Our analysis of  $\eta$  Boo demonstrates the advantages of the QDG method, which can quickly and unambiguously isolate those models whose oscillation spectra closely match the observed spectrum from within a multidimensional grid in mass, age, and metallicity. The success of the method depends on both the quantification of the differences between an observed and model spectrum via our  $\chi^2$  formulation and the existence of a very dense grid of models that allow interpolation between model grid points.

The extensive and detailed grid enables us to study model-to-model variations in the oscillation spectra of stars. The avoided-crossing ridges, for example, are clearly discernible in frequency versus age plots. The first avoided-crossing ridge, in a nonradial oscillation frequency versus age plot, separates modes that are unmixed to the left from modes that are mixed. The frequency spacing between adjacent mixed modes is not as even as for unmixed modes. As we demonstrate for  $\eta$  Boo in this paper, by observing the irregular spacings and their frequency position within the observed spectrum and comparing their positions to the avoided-crossing ridges, one can fine-tune the age determination.

We are looking forward to future seismic observations from *MOST* (Walker et al. 2003; Green et al. 2003) and *COROT* (Baglin et al. 2002). At the time of this writing *MOST* has already begun collecting seismic data on Procyon and is scheduled to collect data on  $\eta$  Boo later in 2004. *COROT* is scheduled to be launched sometime after 2005. With the successful application of even the limited stellar oscillation data obtained from the ground, we hope future satellite missions of increased sensitivity and duration will be proposed to tackle what we believe is the next important step in asteroseismology, the study of the oscillation spectra of stars in clusters.

This work was supported in part by an NSERC grant to D. B. G. The computations were carried out at Saint Mary's University's Institute for Computational Astrophysics.

#### REFERENCES

- Alexander, D. R., & Ferguson, J. W. 1994, *ApJ*, 437, 879  
 Baglin, A., Auvergne, M., Barge, P., Buey, J.-T., Catala, C., Michel, E., & Weiss, W. (*COROT* Team). 2002, in Proc. First Eddington Workshop on Stellar Structure and Habitable Planet Finding, ed. B. Battrick, F. Favata, I. W. Roxburgh, & D. Galadi (ESA SP-485; Noordwijk: ESA), 17  
 Bahcall, J. N., Pinsonneault, M. H., & Basu, S. 2001, *ApJ*, 555, 990  
 Bahcall, J. N., Pinsonneault, M. H., & Wasserburg, G. J. 1995, *Rev. Mod. Phys.*, 67, 781  
 Brown, T. M., Kennelly, E. J., Korzennik, S. G., Nisenson, P., Noyes, R. W., & Horner, S. D. 1997, *ApJ*, 475, 322  
 Christensen-Dalsgaard, J., Bedding, T. R., & Kjeldsen, H. 1995, *ApJ*, 443, L29  
 Di Mauro, M. P., Christensen-Dalsgaard, J., Kjeldsen, H., Bedding, T. R., & Patern, L. 2003, *A&A*, 404, 341  
 Green, D., Matthews, J., Seager, S., & Kuschnig, R. 2003, *ApJ*, 597, 590  
 Guenther, D. B. 1994, *ApJ*, 422, 400  
 Guenther, D. B., & Brown, K. I. T. 2004, *ApJ*, 600, 419  
 Guenther, D. B., & Demarque, P. 1996, *ApJ*, 456, 798  
 Guenther, D. B., Demarque, P., Kim, Y.-C., & Pinsonneault, M. H. 1992, *ApJ*, 387, 372  
 Iglesias, C. A., & Rogers, F. J. 1996, *ApJ*, 464, 943  
 Kjeldsen, H., et al. 2003, *AJ*, 126, 1483  
 Morel, P., & Thévenin, F. 2002, *A&A*, 390, 611  
 Richer, J., Michaud, G., & Turcotte, S. 2000, *ApJ*, 529, 338  
 Rogers, F. J. 1986, *ApJ*, 310, 723  
 Rogers, F. J., Swenson, F. J., & Iglesias, C. A. 1996, *ApJ*, 456, 902  
 Scuflaire, R. 1974, *A&A*, 36, 107  
 Sills, A., & Deliyannis, C. P. 2000, *ApJ*, 544, 944  
 Unno, W., Osaki, Y., Ando, H., & Shibahashi, H. 1989, *Nonradial Oscillations of Stars* (2d ed.; Tokyo: Univ. Tokyo Press)  
 Walker, G., et al. 2003, *PASP*, 115, 1023